Micro-Particles Dispersion and Gas Dynamics in an Axi-Symmetric Supersonic Nozzle

S. M. Soliman*, S. Abdallah, E. J. Gutmark and M. Turner
Dept. of Aerospace Eng. and Eng. Mechanics, PO Box 210070
University of Cincinnati, Cincinnati, OH 45221

Abstract

This paper describes a new pain free device for micromolecular vaccine/drug delivery. The device accelerates micro solid particles to high speeds sufficient to penetrate the epidermis/dermis layer to achieve the pharmaceutical effect (cells of interest). Helium is used as the driving gas for the solid particles because of its high compressibility factor. Numerical parametric study for gas pressures ranging between 3 and 6 MPa and gold particles of diameters 1.8 μm and 5 μm is investigated. The computed results using FINE/Turbo show that uniform particle velocity was achieved at standoff distance of 20 mm downstream of the device exit with particles concentrated on the supersonic core jet. Changing the helium pressure did not change the particles velocity but increased the gas velocity by about 16 %. Furthermore gas pressure has no effect on the particles concentration at device exit. The calculated Particle impact parameter required to insure particle penetration to breach stratum corneum was achieved for both 5μm and1.8 μm gold particles with the later has more uniform spatial distribution.

* Corresponding author

Nomenclature

A	particle projected area (m^2)
d	penetration depth (μm)
D	total drag force acting on the particle
F_i	resistive inertial force of the target material
F_f	frictional resistive force
F_y	yield force
K	Von Karman constant, used for inner layer ≈0.41
L_{ref}	reference length of the test case (m)
M	Mach number
M	mass (kg)
M	Mass flow rate (Kg/s)
P	Pressure (Pa)
r_p	radius of the particle (μm)
V	velocity (m/s)
V_i	impact velocity of the particle (m/s)
V_{ref}	reference velocity of the flow, for instance the inlet velocity (m/s)
y^+	non-dimensional value
y_{wall}	the distance of the nearest grid point to the wall (m)
ρ_p	density of the particle (kg/m^3)
ρ_t	the target material density (kg/m^3)
ν	kinematic viscosity of the fluid (m^2/s)
ν_t	turbulent kinematic viscosity (m^2/s)
Φ	Dissipation function.

Introduction

Traditional needles have several disadvantages including accidental needle-sticks, pain and needle phobia. Thus the search for needle free drug/vaccine delivery has been accelerated by recent decades. Powder injectors, liquid jet injectors, microneedles and thermal microablation are the most recent trends for micro molecular drug/vaccine delivery. Recent drug delivery techniques have many advantages over the traditional ones, e.g. pain free, easiness, mass vaccination, safety and cost [1-5].

Drug/vaccine delivery by means of powder injections may eradicate the necessity of the cold chain, which should further decrease the cost of vaccine delivery [1, 2, 6, 7]. The "Cold Chain" is all means of transporting and storing vaccines/DNA within their proper storage temperature. It starts with production processes, transportation and ends with the local immunization provider.

Powder injections can be utilized by means of the biolistic device/gene gun. It has many applications, e.g. human genetic immunization, cancer gene therapy and vaccination as well as many plant applications through injecting micro particles to the cells of interest. The micro particles gain its momentum from the gas flow which is derived by compressed gas. The particles momentum should be sufficient to penetrate the skin to the cells of interest. Because of many limitations for experimental work to use humans/animals, cost etc… Particle impact parameter is the key measure for achieving certain depth below skin. It has been proved the direct relation between the particle impact parameter and the depth of penetration [3, 8]. The particles must have uniform velocity distribution and uniform concentration to insure the pharmaceutical effect. Generally a penetration depth of approximately 20–100 μm should be achieved to pledge epidermal drug delivery [9].

Powder injection Technology was originally developed in the area of plant genetics to launch gene into target cell. Stanford et al [10] designed and constructed a particle accelerator device which could accelerate small particles to a velocity sufficient to penetrate cell walls and membrane in a non lethal manner. Blowers et al [11] insert modified DNA/RNA into algal. Oard J. H., et al [12] used the gene-gun which was originally designed to propel DNA-coated gold particles (using exploding gunpowder as an accelerant) through plant cell walls. High pressure helium replaced gunpowder in most particle-mediated delivery devices [13, 14]. The method is also applied to deliver genes into mammalian cells [15].

Kuriyama, S., et al, [16] developed gene gun, in which microprojectiles are discharged using a hammering bullet. They used it to inject gold particles coated with lacZ expression plasmid to murine livers.

Bellhouse et al., [17] developed a hand held needle-free jet-propelled particle injection system for injecting solid micro particles, many amendment to the same device followed by Kendall et al [18-21], and Liu et al [22-34]. They used two techniques to deliver the microparticles into the human skin or mucosal tissue 1) Using a supersonic Converging–Diverging nozzle (C-D nozzle) 2) Using a contoured shock-tube (CST). One of the major parameter controlling the effectiveness of transmitting vaccines/drugs is the uniformity of particle velocity versus the radial position; Liu et al [34] found that moderate swirl ratio (e.g. 30 %) result in uniform gas and particle velocity for SFD particles of 45 μm.

Lin H. J., et al [35], developed A low pressure gene gun to decrease the noise and cell damage caused by high-pressure gene guns. This device can introduce gold particle-coated DNA into animal cells using supersonic flow generated by a rocket nozzle.

In this paper we studied the effect of changing the driver pressure, particle diameter, adding swirl for

uniformity of the particle velocity, particle impact diameter, and number concentration at device exit.

Physical Model

In this paper, we propose a model device which consists of 1) Helium gas tank (not simulated here) regulated by pressure regulator 2) inlet disk which fed by the gas tank 3) C-D nozzle followed by cylindrical section 3) diverging section followed by second cylindrical section 4) second diverging section as shown in Fig. 1.

The supersonic C-D nozzle has a throat diameter of 1.4 mm and area ratio 9. The C-D nozzle is followed by two constant area section and two divergent sections alternately compromising the second nozzle. The exit nozzle diameter is 10 mm while the overall area ratio is about 51. The values of these parameters, illustrates the complexity of the flow field inside the device.

The c-d nozzle distinguishes this model from the model by Liu et al [34], where a convergent section followed by a cylindrical part causing a jump in geometry (back step). The back step is known to provide several computational challenges, the most notable of which, is the difficulty of the numerical solution to converge due to high-pressure gradients. Moreover [34] used gas tank which restricts the multi-use of the device. Flow field will bean transient starting from high pressure, consequently high particle velocity and decreased till it reaches ambient conditions. The particles carried by the flow field after certain time will not have the sufficient momentum to penetrate to the required skin layers. In our model we propose to use a high pressure compressed gas tank with pressure regulator to maintain delivery of gas at constant pressure. The high-pressure helium initially stored in the gas-tank and controlled by pressure regulator insures the steadiness of the flow field along the device.

The user may change the operating pressure through changing the driver pressure by the regulator depends on the kind of microparticles e.g. tungsten, gold, polystyrene or any other biological inert particles. When the compressed gas enters into the inlet disk and aligns itself with contours of the c-d nozzle. Consequently, a supersonic streamwise vortex is generated inside the nozzle. This vortex then interacts with the shock system already in the conical nozzle while operated in a large pressure ratio. This interaction between the supersonic streamwise vortex and the shock wave is a natural extension of the vortex breakdown problem, which can significantly affect the aerodynamic performance characteristics of our device. Micro-particles enter the mainstream flow at inlet and accelerate towards the conical nozzle exit. The particles, with their relatively large inertia, maintain a high momentum and target the cells of interest. The introduction of the swirl aims to distribute the micro-particles to a larger area and achieve a more uniform impact velocity.

The design of the swirl components largely depends on extensive experimental work to achieve the desired delivery efficiency and penetration depth. Given the enormous number of parameter variations involved in the simulation process, the trial and error approach is very expensive and time consuming. Furthermore, a relatively small space (e.g. the radius of the c-d nozzle throat, 0.7 mm) in addition to the practical challenges. Advanced CFD simulation codes lend us an efficient and accurate tool of modeling these sophisticated supersonic swirl flows and thus, it is highly desirable to develop modules, to be incorporated in CFD codes that help guide the optimization of swirl component designs.

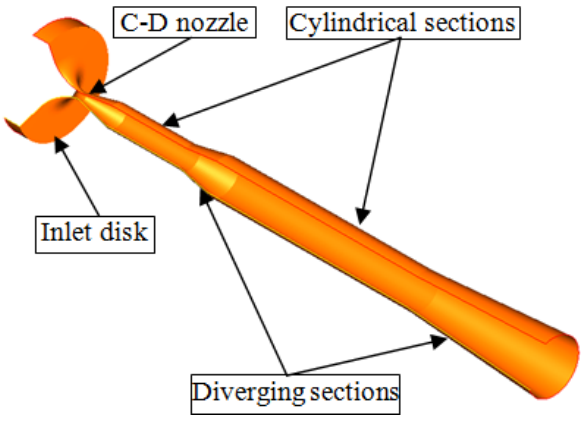

Figure 1. Our Nozzle Physical model.

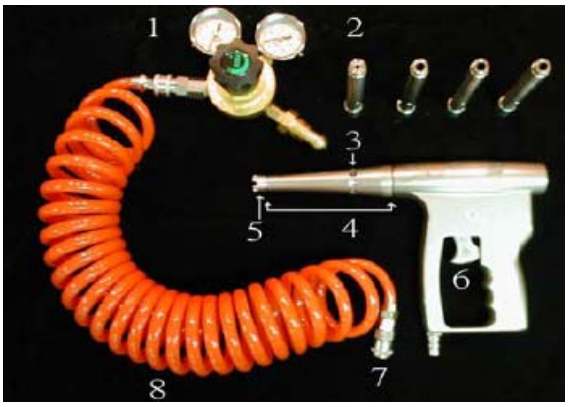

Figure 2. BioWare low-pressure gene gun. (http://www.bioware.com.tw/bioware/BIOWARE%20-e/products/products-gene%20gun.htm).

Numerical method

Commercial CFD software, NUMECA's FINE/Turbo is used to numerically simulate the gas and particles flow of the proposed device. Because of the high Reynolds Number (≈ $1.8\text{x}10^5$), there is a possibility of little disturbances caused by the pressure gas regulator and surface roughness of the device walls; Spalart-Allmaras (1-equation model) is used to precisely predict the turbulence quantities of the flow-field behavior with a good rate of convergence [36]. A second order accuracy is satisfied to accurately predict the interaction between the oblique shock and the turbulence boundary layer. Helium gas is utilized as the driving gas at different pressures and room temperature. Atmospheric pressure is specified as the outlet boundary condition for the subsonic upstream flow. The device walls are assumed adiabatic during the particle delivery time usually < 5 ms of interest [22, 34], with a non-slip velocity condition imposed at the walls. The external boundary condition is set for the far field boundaries.

Estimation of the kinematic turbulent viscosity as an inlet condition is based on the following assumption as given in [37]:

$$\frac{\upsilon_t}{\upsilon} = 1 \text{ to } 5 \qquad (1)$$

The Spalart-Allmaras model has been chosen for the flow field simulation because of its robustness and the lower additional CPU and memory usage compared to the k-**ε** and Baldwin-Lomax models. Spalart-Allmaras model is based on the resolution of an additional transport equation for the eddy viscosity. The equation contains an advective, a diffusive and a source term and is implemented in a non-conservative manner. The governing equations, closure coefficients and functions are given in references [36, 37].

Reynolds Averaged Navier-Stokes Equations (RANS)

The randomly changing flow variables in conventional Reynolds decomposition is replaced by two parts: 1) a steady quantity time average, and 2) its fluctuation quantity. More details about turbulent decomposition, different forms for RANS and boundary layer equations are available in references [36-38]. The turbulent flow governing equations for mass-weighted variable are given as [36]:

$$\text{Continuity} \qquad \frac{\overline{\partial \varrho}}{\partial t} + \frac{\partial}{\partial x_j} = 0 \qquad (2)$$

$$\text{Momentum } \frac{\partial}{\partial t}(\bar{\varrho}\,\tilde{u}_i) + \frac{\partial}{\partial x_j}\left(\bar{\varrho}\,\tilde{u}_i\,\tilde{u}_j\right) = -\frac{\partial P}{\partial x_i} + \frac{\partial}{\partial x_j}\left(\bar{\tau}_{ij} - \overline{\varrho\,\acute{u}_i\,\acute{u}_j}\right) \qquad (3)$$

The energy equation in terms of static temperature is given as:

$$\frac{\partial}{\partial t}\left(\bar{\varrho}\,c_p\,\tilde{T}\right) + \frac{\partial}{\partial x_j}\left(\bar{\varrho}\,c_p\,\tilde{T}\,\tilde{u}_j\right) = \frac{\partial \bar{P}}{\partial t} + \tilde{u}_j\frac{\partial \bar{P}}{\partial x_j} + \overline{\acute{u}_j\frac{\partial P}{\partial x}} + \frac{\partial}{\partial x_j}\left(k\frac{\partial \tilde{T}}{\partial x_j} + k\frac{\partial \bar{T}}{\partial x_j} - c_p\,\overline{\varrho\,\acute{T}\,\acute{u}_j}\right) + \bar{\phi} \qquad (4)$$

Computational domain and Boundary conditions

Because of the complexity of the device geometry, the grid consists of five blocks, three of which fitted well along the device and the other two are placed outside, these blocks are extended to 285d axially and 71d in the radial direction (where d is diameter of the sonic throat), to accommodate the external boundary condition as shown in Fig. 3. To provide grid independent results for turbulent flow as well as a good resolution of the flow field, the mesh is denser in the regions of interest, like in the turbulent boundary layer and near the center of the device to capture the shock waves interaction. The grid is also dense across the geometrical corners to capture the concentrated high flow field gradients. The numbers of points along each segment of each block are chosen carefully to satisfy at least 3 multigrid levels to insure the grid-independence requirement. The total number of points in the coarse grid level is 44652 points, 32330 points of which are placed inside the device and the rest is placed outside. The number of nodes along the diameter is taken to be 61, for multigrid purposes, 19 nodes of which are placed near the wall across the boundary layer, while 505 cells are placed along the axis of the device for better resolution of the flow field.

Despite the fact that the area of the c-dnozzle is small compared to the total area of the device, it actually controls the flow field. Hence, one block is especially constructed for this area with 8906 total number of points.

The quality of the flow solution often depends upon the capture of the flow phenomena inside the boundary layers which developing along the solid walls. FINE/Turbo recommends locating the nearest grid point along the wall at a distance that corresponds to parietal coordinate y+ ranging from 20-50 for high Reynolds number models [37].The truncated series solution for turbulent flows of the Blasius equation is used to estimate the width of the first cell close to the wall y_{wall}. By substituting the average velocity at the nozzle exit and the characteristic length of the device

into Eq. 5, we get the first cell distance from the wall to be equal to 10 µm which corresponds to Y^+ of 40.

$$y_{wall} = 6\left(\frac{V_{ref}}{\upsilon}\right)^{-\frac{7}{8}}\left(\frac{L_{ref}}{2}\right)^{\frac{1}{8}} Y_1^+ \qquad (5)$$

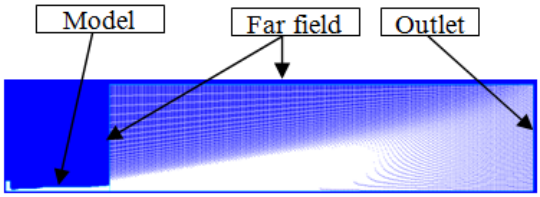

Figure 3. Computational domain and boundary conditions.

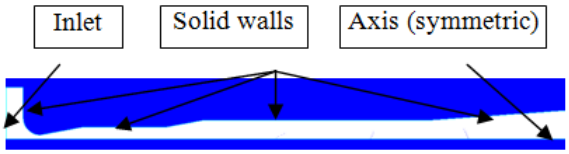

Figure 4. Device boundary conditions.

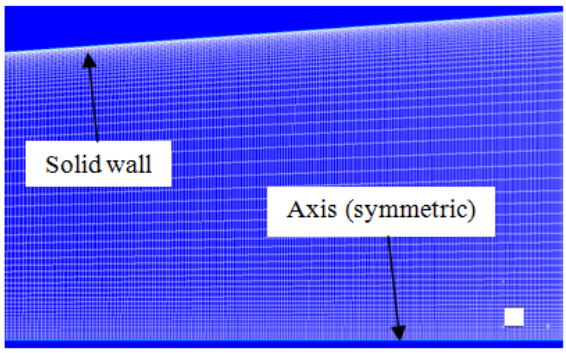

Figure 5. Cross-section zoomed near walls

Results and Discussion

Model Validation

The numerical model suggested by Yi. Liu et al [34] were used for validation. Yi Liu et al [34] have used different CFD code to capture the particle/gas dynamics. They carried out parametric study to determine the optimum swirl ratio for SFD particles for optimum particle velocity distribution. A baseline 4 MPa driver gas pressure was used to initialize the flow field which we used in our model for validation purpose. Comparison of velocity magnitude contours are shown in Fig. 6. Furthermore convergence criteria for different operating pressure; mass flow rate and global residuals were monitored. The residuals for all cases were decreased more than three orders of magnitude and the mass flow rate difference was less than 0.5 % as shown in Table 1.

Convergence criteria	Mass flow rate (g/s)			Global residuals
	Inlet	outlet	Error %	
3 MPa	3.343	3.337	0.159	> 3
4 MPa	5.794	5.786	0.132	> 3
5 MPa	7.244	7.238	0.074	> 3
6 MPa	8.694	8.685	0.099	> 3

Table 1. Convergence criteria

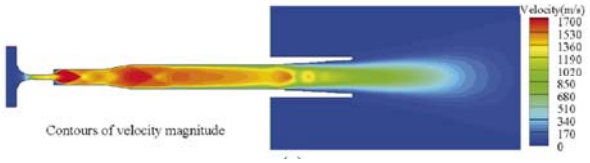

Figure 6. Velocity magnitude contours from [34]

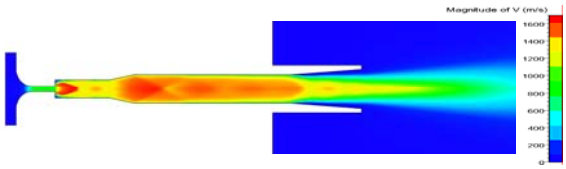

Figure 7. Velocity magnitude contours.

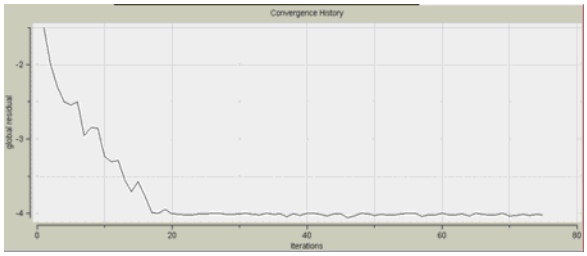

Figure 8. Global residual monitor.

Simulation with different Driver gas pressure

The simulation was done first using different driver gas pressure ranging from 3 to 6 MPa. Axial gas velocity results are shown in Fig. 9, while the Mach contours are shown in Fig. 10. As we expected the nozzle is choked, the gas reaches sonic velocity at the throat for all cases. Oblique shocks are observed at the

beginning of first and the second constant area section. The gas axial velocity is increasing towards device exit, thus the velocity at the first diverging section is lower than the velocity at the end of the second diverging section consequently the second oblique shock is much stronger than the first one as shown in Fig. 10. Increase driver gas pressure extends the supersonic core jet as shown from Fig. 13. By analysis of Fig. 12 we confirm that the gas axial velocity at the exit increase as the driver gas pressure increases. The gas axial velocity is maximum at the center and decreased towards the walls of the device confirms the no slip condition at the walls but separation noticed for all cases at the last diverging section near the device exit due to adverse pressure near the walls at this section as shown in Figs. 11-12.

The fact that there is a separation is clearly shown at Fig. 11 which shows the velocity vectors near the walls. The separation starts at the end of the cylindrical section and grows towards the exit till it reaches maximum at the mid-section of the diverging section, then it starts to decrease towards the exit. The gas axial velocity is more uniform at the end of the second cylindrical part and changes to parabolic trend as it travels through the last diverging section.

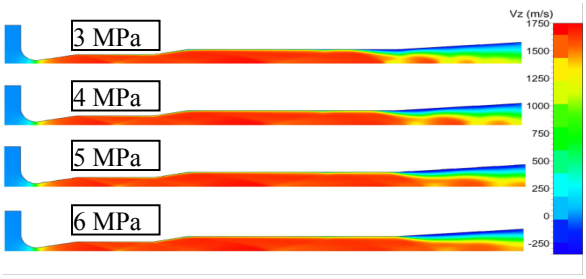

Figure 9. Gas axial velocity contours for different driver pressure.

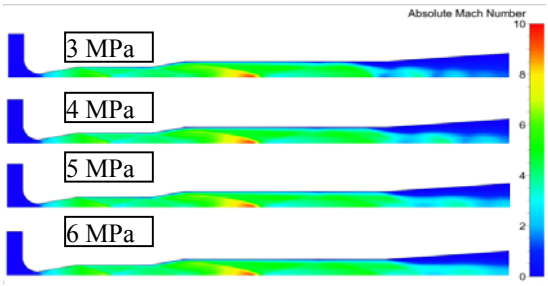

Figure 10. Gas Mach number contours.

Figure 11. Velocity vector near the device exit.

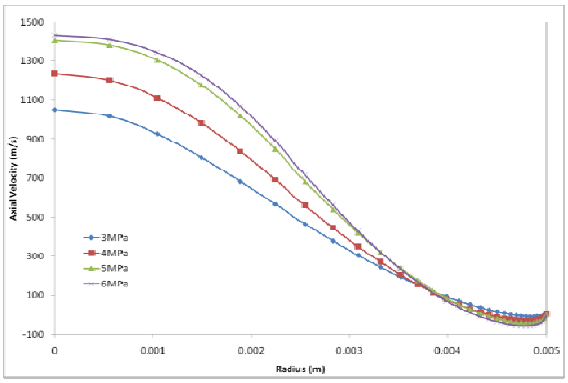

Figure 12. Gas axial velocity at nozzle exit.

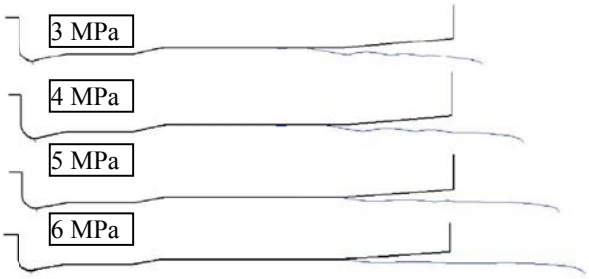

Figure 13. Sonic line for different pressure

Simulation with different Particle diameter

The device presented here in this paper is intended to be used for Cancer Therapy, Vaccination, and immunization through injecting DNA to the live cells targeting epidermis or dermis cells. DNA cannot penetrate the human skin by itself. The biologically inert particles e.g. gold or tungsten are used for this purpose through coating these micro particles with DNA [40-41].

Here we introduce gold particles with diameters 1.8 and 5 Micrometer (density 19,320 kg/m^3) to the flow field from the inlet. Both types of gold particles are simulated at different pressure to study the effect of driver gas pressure on the particle dynamics.

Gas axial velocity at device exit for different driver gas pressure is shown in Fig. 14. The gas velocity has the same trend similar to the gas velocity without particles except near the walls of the device where the turbulent boundary layer exist as illustrated in Fig. 15. The Particle axial velocity for the different driver gas pressure has almost the same trend and magnitude at device exit as shown in Fig. 16 probably because the particles is still gaining momentum from the gas even after it leaves the device exit as shown in mass-weighted velocity contours for 6 MPa driver pressure as shown in Fig. 18.

The particle mass-weighted average velocity reaches its maximum at 20 mm downstream of the device exit and it increased by ≈ 13 % more than its value at exit for 6 MPa case as shown in Fig. 17. Similar results obtained for the other driver pressures. Consequently it is advised to use the device at this distance from the skin for better results. This distance called stand-off distance and is defined as the distance that the particles travels after leaving the device till it reaches the skin. Yi Liu et al [30] study the effect of this distance on the particle performance ranging from 2: 15 mm which depends on driver gas pressure and particles physics i.e. diameter and density.

Particle velocity is clearly lower than the gas velocity due to particle drag force. By analysis of Fig. 19, it is clear that the exit velocity for the 1.8 µm is about three times higher than the case done using 5 µm as expected because of the higher drag affected the particles in case of higher particle diameter then the smaller particle diameter. Moreover the 1.8 µm has more spatial distribution.

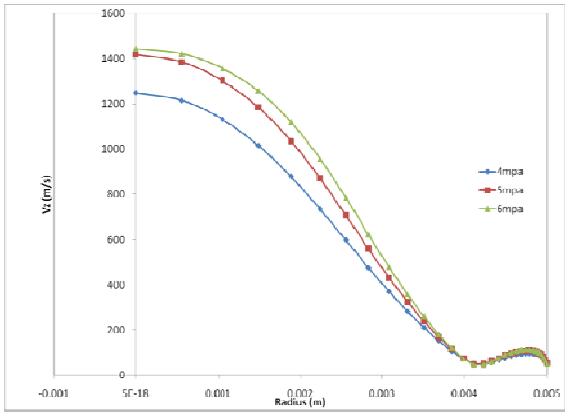

Figure 134. Gas axial Velocity at nozzle exit with particles.

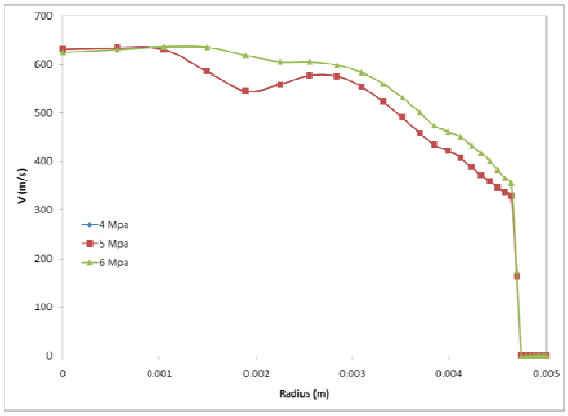

Figure 156. Particle Axial Velocity at device exit (1.8 µm).

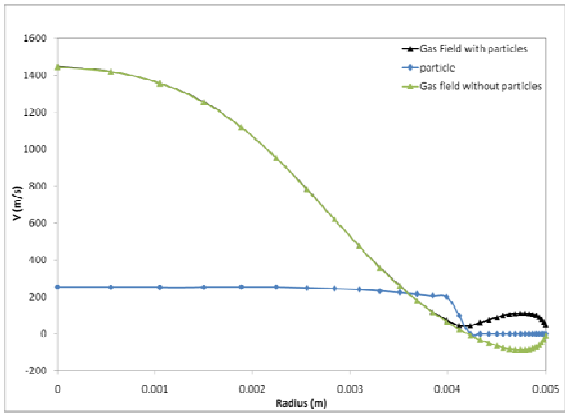

Figure 145. Gas and particles axial velocity (6 MPa, 5 µm Particles).

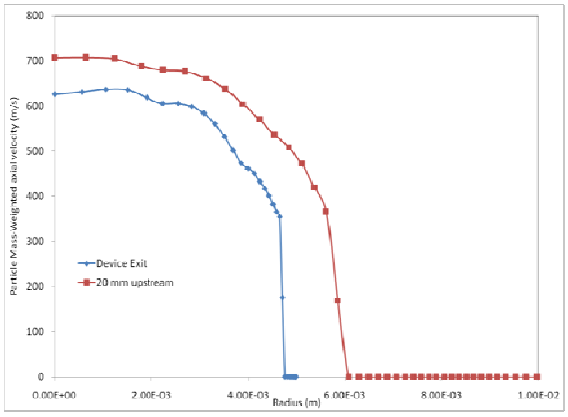

Figure 167. Particle mass-weighted axial velocity comparison (case 6 MPa, 1.8 µm).

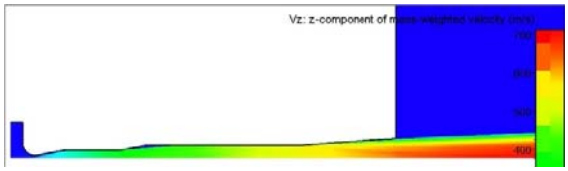

Figure 178. Mass-weighted velocity contours (6 MPa).

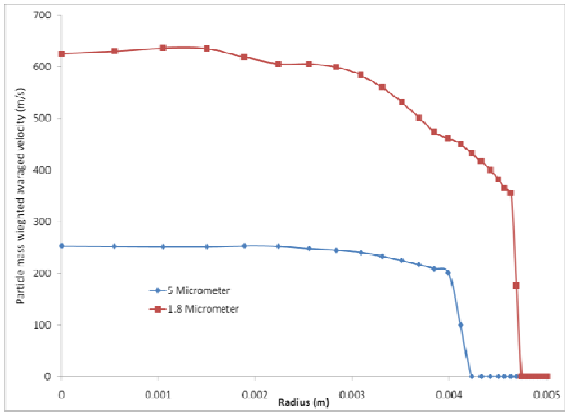

Figure 189. Particle mass-weighted averaged velocity at device exit.

Particle Impact Parameter (PIP)

PIP is defined as the product of particle density by particle radius and particle velocity. It has been proved that it is proportional to the penetration depth in skin. PIP of approximately 7 kg/m.s is required for particles to begin breach the stratum corneum but 12 kg/m.s is requisite if all the impacting particles are to breach the stratum corneum [28].

$$PIP = \rho_P r_P v \quad (6)$$

Calculation of PIP prove that micro-particles of both diameters have PIP sufficient to cause the Pharmaceutical effect for driver pressure 4 MPa or more, as we increase the pressure the effective area increased. The optimum pressure for both diameters is 5 MPa in which both have sufficient PIP and greater area as shown in Fig. 20. Micro-particles of smaller diameters have a larger effective area more than the ones which have bigger diameters.

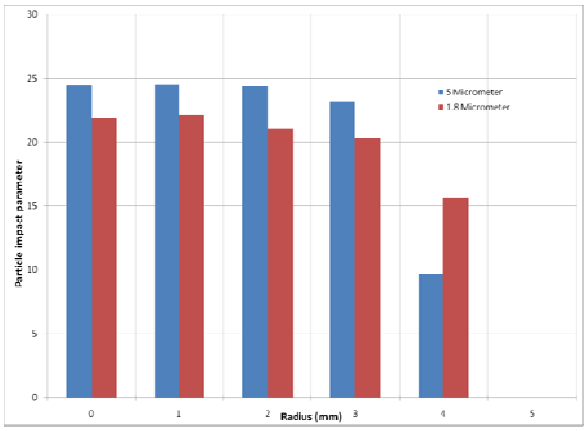

Figure 19. Particle impact parameter (5 MPa).

Conclusion

We developed and numerically tested a new pain free device for micromolecular vaccine/drug delivery to human skin. The device consists of two C-D nozzles to accelerate drug carrier particles using helium gas to supersonic speeds. Numerical testing of the device shows that it achieves pharmaceutical effect for both cases 1.8 and 5 μm if the device driver pressure is 4 MPa or higher. The computational model was validated by reduplicating some of the existing state of the art numerical results using FINE/Turbo code. The computed results of our model using the same code are obtained using 44652 grid points for unsteady turbulent flow. Residual convergence of four orders of magnitude and mass difference between inlet and exit of less than 0.5 % confirm the accuracy of the computed results. Several parametric studies were done to optimize the operating conditions of the device.

References

[1] E. L. Giudice, and J. D. Campbell. *Advanced Drug Delivery Reviews,* 58:68-89, 2006.

[2] M.A. Kendall, T. J. Mitchell, G. Costigan, et al. *The Journal of Allergy and Clinical Immunology*, 117:275-282, 2006.

[3] A. Aroraa, M. R. Prausnitzc, S. Mitragotri. *International Journal of Pharmaceutics,* 364:227-236, 2008.

[4] D. N. Tarala. *Journal of Biosciences; Dordrecht,* 34: 995-1003, 2009.

[5] M. B. Brown, G. P. Martin, S. A. Jones, et al. *Drug delivery,*13:175-187, 2006.

[6] H. J. Dean, and D. Chen, *Vaccine,* 23:681-686, 2004.

[7] M. M. Levine, *Nature Medicine; New York*, 9:99-103, 2003.

[8] T. J. Mitchell, M. A. Kendall, and B. J. Bellhouse, *International Journal of Impact Engineering*, 28:581-599, 2003.

[9] A. S. Ziegler, *Journal of Pharmaceutical Innovation,* 3:204-213, 2008.

[10] J. C. Sanford, T. M. Klein, and E. D. Wolf, *Particulate Science and Technology,* 5:27-37, 1987.

[11] A. D. Blowers, L. Bogorad, H. B. Shark, J. C. Sanford. *The Plant Cell*, 1:123-132, 1989.

[12] J. H. Oard. *Plant Physiology*, 92:334-339, 1990.

[13] N. S. Yang, J. Burkholder, B. Roberts, B. Martinell, and D. Mccabe. Proc. Natl. Acad. Sci. USA, 87: 9568–9572, 1990.

[14] N. S. Yang, and P. Christou, *Particle Bombardment Technology for Gene Transfer*, *Oxford University Press*, 1994.

[15] W. C. Heiser. *Analytical Biochemistry*, 217:185–196. 1994.

[16] S. Kuriyama, A. Mitoro, H. Tsujinoue, et al. *Gene Therapy*, 7:1132-1136, 2000. .

[17] B. J. Bellhouse, D. F. Sarphie, and J. C. Greenford. *Needless Syringe Using Supersonic Gas Flow for Particle Delivery*, Int. Patent US5899880, (1994).

[18] M. A. Kendall. *Journal of Investigative Dermatology,* 122:739-746, 2004.

[19] M. A. Kendall, T. Mitchell, and P. Wrighton-Smith. *Journal of Biomechanics,* 37:1733-1741, 2004.

[20] M. A. Kendall, *Vaccine,* 24:4651-4656. 2006.

[21] M. A. Kendall. *Proceedings of the Fifth International Conference on CFD in the Process Industries, Melbourne, Australia*, 13-15 December, 2006.

[22] Y. Liu, M. A. Kendall, and N. Truong. *20th AIAA Applied Aerodynamics Conference, Saint Louis, MO, UNITED STATES*, 2002.

[23] Y. Liu, G. Costigan, and B. J. Bellhouse. *35th AIAA Fluid Dynamics Conference and Exhibit,* pp.1-11, *Toronto, Ontario, Canada, June* 2005.

[24] Y. Liu, and M. A. Kendall. *Biomedical Microdevices,* 8:341-351, 2006.

[25] Y. Liu. *Physica D,* 237:233-242, 2008.

[26] Y. Liu. *Biotechnology,* 5:42-48, 2006.

[27] Y. Liu. *Medical & Biological Engineering & Computing,* 44:551-559, 2006.

[28] Y. Liu, and G. Costigan. *24th Applied Aerodynamics Conference*, San Francisco, California, June 2006.

[29] Y. Liu, *IEEE Transactions on Biomedical Engineering,* 54:1814-1821, 2007.

[30] Y. Liu, N. K. Truong, and M. A. Kendall. *Biomedical Microdevices,* 9:465-474, 2007.

[31] Y. Liu. *IEEE Transactions on Biomedical Engineering,* 54:1507-1521, 2007.

[32] Y. Liu. *Medical Engineering & Physics,* 29:390-397, 2007.

[33] Y. Liu, and M. A. Kendall. *Biotechnology and Bioengineering,* 97:1300-1308, 2007.

[34] Y. Liu, G. Costigan, and B. J. Bellhouse. *Powder Technology,* 183:189-195, 2008.

[35] H. J. Lin, et al. *Low pressure accelerated particle gene gun*, US Patent US6436709, 2002.

[36] J. C. Tannehill, D. A. Anderson and R. H. Pletcher. *Computational Fluid Mechanics and Heat Transfer*, 2nd ed., Taylor & Frances, 1997.

[37] NUMECA, "FINE/Turbo user's guide volume.

[38] F. M. White. *Viscous Fluid Flow*, McGraw Hill, New York, 1991.

[39] J. T. Dehn. *Unified Theory of Penetration," Army Ballistic Research Lab.*, BRLTR2770; ADA1762491, Aberdeen Proving Ground, MD; United States, 1986.

[40] D. Chen, Y. F. Maa, and J. R. Haynes. *Expert Rev. Vaccines,* 1: 265–276, 2002.

[41] C. Lin, and M. Yen. *The Journal of Gene Medicine*, 10:679-689, 2008.